J Mater Sci (2009) 44:6310–6316
DOI 10.1007/s10853-009-3869-x

Preparation of $K_2Ti_6O_{13}/TiO_2$ bio-ceramic on titanium substrate by micro-arc oxidation

Zhongwei Zhao · Xingyu Chen · Ailiang Chen · Guangsheng Huo · Honggui Li

Received: 19 June 2009 / Accepted: 3 September 2009 / Published online: 15 September 2009

Abstract $K_2Ti_6O_{13}/TiO_2$ bio-ceramic coatings are prepared successfully by micro-arc oxidation on titanium substrate in pure KOH electrolyte solution. The coating is prepared at various applied current density (150–500 mA/cm^2) and in KOH electrolyte with different concentrations (0.5–1.2 mol/L). The composition and surface morphologies of coatings are strongly dependent on the applied current density and the electrolyte concentration. On the condition of lower current density and electrolyte concentration, $K_2Ti_6O_{13}$ phase almost cannot be formed. The phase is mainly composed of rutile and $K_2Ti_6O_{13}$ with increasing current density and electrolyte concentration. The surface morphologies are composed of whiskers and porous structures. The ability of $K_2Ti_6O_{13}/TiO_2$ bio-ceramic films inducing apatite deposition is evaluated by soaking it in biological model fluids. The results show the $K_2Ti_6O_{13}/TiO_2$ bio-ceramic coatings possess excellent capability of inducing bone-like apatite to deposit.

Introduction

Currently titanium and its alloys are widely used as implants materials due to its good mechanical and anti-corrosive properties and excellent biocompatibility [1–3]. However, bone tissue cannot well bond with the surface of titanium or titanium alloys because of their poor bioactivity and osteoinductive properties [4–6]. To improve the bone bonding ability of titanium implants, titanium surface needs to be modified to prepare a layer of coatings possessing good bioactivity [7, 8]. After modification, titanium substrate composite materials possess not only the good mechanical and anti-corrosive properties but also the excellent biocompatibility and good bioactivity [9, 10].

Many kinds of bioactive coatings, such as hydroxyapatite [11], calcium phosphate ceramics [12], $CaTiO_3$, and TiO_2 coatings [13], can be prepared on the titanium substrate surface. Potassium titanate ($K_2Ti_6O_{13}$) possesses excellent biocompatibility [14] and good bioactivity properties due to its special structure, composition, and physical–chemical properties [15]. So the $K_2Ti_6O_{13}$/Ti composite materials will be a kind of excellent implant materials [16]. Recently, several methods for preparing $K_2Ti_6O_{13}$ coatings on titanium substrate have been reported. For instance, Cui Chunxiang et al. [16] obtained $K_2Ti_6O_{13}$ bio-ceramic coating on the surface of titanium alloy using an in situ kneading-drying-calcination synthesis technique, and Kokubo [17] prepared $K_2Ti_6O_{13}$ coating on titanium substrate by KOH and heat treatments. In the two methods, besides complex process, titanium substrate must be treated at very high temperature. After heat treatment with high temperature, the structure of titanium and its alloys will be changed, which will affect the properties of titanium used as the implant materials.

Micro-arc oxidation (MAO, also named as plasma electrolytic oxidation or anodic spark oxidation), a particularly interesting process, can produce a porous, relatively rough, and firmly adherent oxide film on valve metals such as Al, Ti, Mg, and Zr [18, 19]. The porous nature of anodized films can enhance the implants' anchorage to the bone and give rise to the possibility of the incorporation and the release of antibiotics around the titanium implants [20, 21]. By applying positive current to Ti specimen immersed in electrolyte, anodic oxidation (or anodizing) of Ti occurs and a TiO_2 layer is formed on the surface. When

Z. Zhao (✉) · X. Chen · A. Chen · G. Huo · H. Li
School of Metallurgical Science and Engineering, Central South University, Changsha 410083, China
e-mail: zhaozw@mail.csu.edu.cn; csucxy@yahoo.com.cn

the voltage increase to a certain point, some micro-arc discharges occur as a result of the dielectric breakdown of the TiO_2 layer [20]. During the process of dielectric breakdown, a series of chemical reactions, electrochemical reactions, and plasma-chemical reactions occur on the titanium surface [22, 23]. In the center of dielectric breakdown, TiO_2 film is melted by spark discharge's high temperature in very short time. At the same time, the melting TiO_2 reacts with a large amount of injected electron and ions diffused from electrolyte, and a new coating is formed on titanium substrate.

In this study, the MAO technique is used to prepare the $K_2Ti_6O_{13}/TiO_2$ bio-ceramic coating on the titanium substrate in the electrolyte of KOH solution. In order to evaluate the biological properties, the $K_2Ti_6O_{13}/TiO_2$ bio-ceramic coatings are soaked in the biological model fluids for several days.

Materials and methods

Preparation of MAO films

The pure titanium plates with the size of $10 \times 10 \times 0.3$ mm^3 are used as the substrate for MAO. The plates are polished to a mirror finish with metallographical abrasive paper and then cleaned with distilled water. The electrolyte solution is prepared by dissolving reagent-grade potassium hydroxide (KOH) in distilled water. In the experimental process, a piece of titanium plate is used as cathode, and the current of MAO is fixed in the range of 150–500 mA/cm^2 using the direct current power supply. The $K_2Ti_6O_{13}/TiO_2$ bio-ceramic coatings are prepared at the different direct current density and different concentration of KOH solution. After the MAO treatment, the samples are washed with distilled water and then dried at room temperature.

Evaluation of the bioactivity of $K_2Ti_6O_{13}/TiO_2$ bio-ceramic coating

The MAO-treated samples are immersed in biological model fluids with the concentration of Ca and P ions almost equal to those in the human blood plasma. The biological model fluids are prepared, according to Feng et al. [24], by dissolving the reagent-grade 0.0555 g calcium chloride ($CaCl_2$), 0.06 g sodium dihydrogen phosphate (NaH_2PO_4), and 0.0126 g sodium bicarbonate ($NaHCO_3$) in 100 mL distilled water, successively. Each MAO sample is washed with distilled water, and then is soaked in biological model fluids in a plastic vial. The plastic vial is sealed and put in a water-bath at 37 °C. After soaking for different time, the soaked samples are washed with distilled water and dried in the air.

Characterization of samples

The phase components of the samples treated with MAO and soaked in biological model fluids are determined by X-ray diffraction (XRD, Dmax/2550VB+, Rigaku Corporation, Japan) using Cu–K radiation from the 2θ values of 10° to that of 70° at 5°/min of scanning speed. The surface morphology of all samples is observed using scanning electron microscopy (SEM, JSM-5600, JEOL, Tokyo, Japan).

Results and discussion

Effect of electrolyte Concentration

Figure 1 shows the XRD patterns of the surface coating phase of samples, which are prepared in KOH electrolyte with concentration of 0.6, 0.8, 1.0, and 1.2 mol/L at 250 mA/cm^2 of current density, respectively. In lower concentration KOH electrolyte (Fig. 1a), no $K_2Ti_6O_{13}$ phase XRD peak is detected on the coating, which is composed of rutile phase and Ti. Increasing the concentration of KOH electrolyte, the rutile XRD peak intensity becomes stronger, and the $K_2Ti_6O_{13}$ XRD peak begins to appear, while the titanium XRD peak intensity gradually decreases. It is clear that the higher concentration of electrolyte, the more easily dielectric breakdown occurs on titanium substrate. So the rutile phase and $K_2Ti_6O_{13}$ phase can be formed more easily on titanium substrate with increasing concentration of KOH electrolyte. But the $K_2Ti_6O_{13}$ phase and rutile phase XRD peak intensity all decrease when the concentration of electrolyte reaches 1.2 mol/L (Fig. 1d). It can be concluded that the reaction of rutile with KOH is accelerated during the process of MAO when the concentration of KOH electrolyte

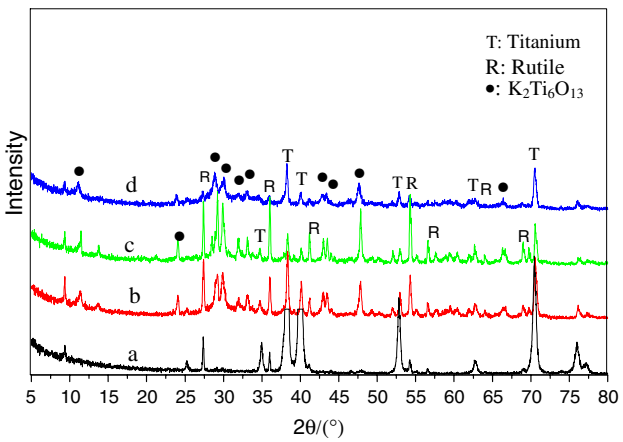

Fig. 1 XRD patterns of the samples oxidized at 250 mA/cm^2 in KOH solution with concentration of (*a*) 0.6 mol/L, (*b*) 0.8 mol/L, (*c*) 1.0 mol/L, and (*d*) 1.2 mol/L

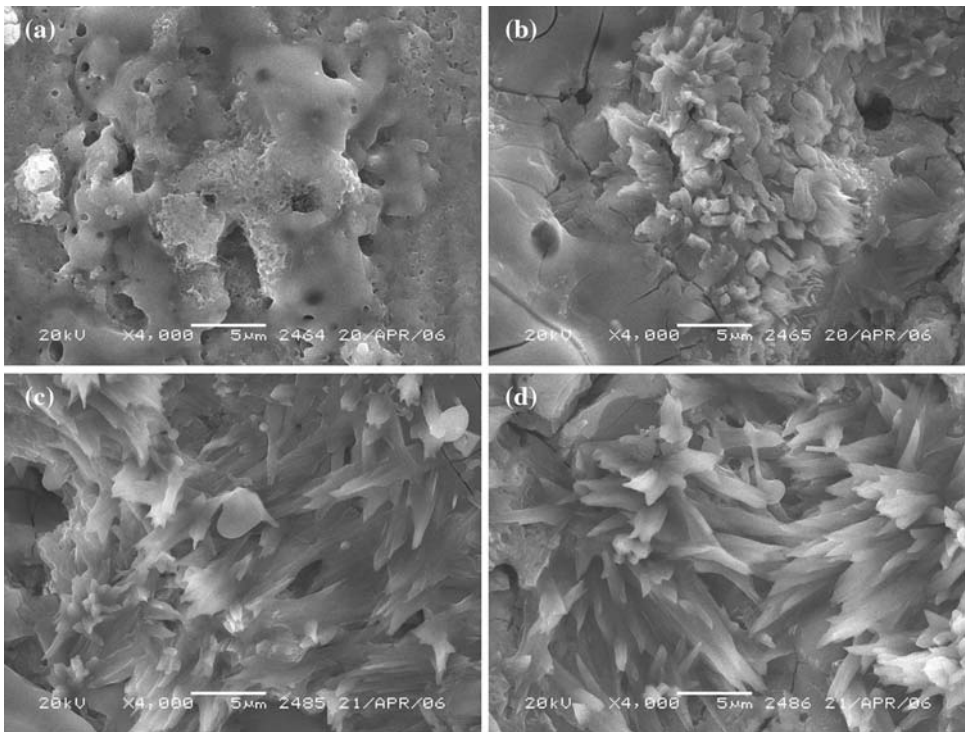

Fig. 2 Surface morphologies of the micro-arc oxidized samples prepared at 250 mA/cm^2 in the KOH of **a** 0.6 mol/L, **b** 0.8 mol/L, **c** 1.0 mol/L, and **d** 1.2 mol/L

increases. So the $K_2Ti_6O_{13}$ phase forms very fast, which can lead to the poor crystallinity of the $K_2Ti_6O_{13}$ phase. Consequently, their XRD peaks intensity is not strong.

Figure 2 is the SEM photographs of the samples prepared in KOH solution with different concentrations. Figure 2a only shows the porous and rough morphologies on the surface of samples. When the concentration of KOH reaches 0.8 mol/L (Fig. 2b), some whiskers structures begin to appear on the surface. With increasing concentration of KOH solution, the whisker structure becomes denser and longer.

The effect of electrolyte concentration on the surface voltage is showed in Fig. 3. From the figure, all voltage–time relations are all serrate curves. The resistance of coating will change with time during the process of dielectric breakdown. So the voltage–time relations are not smooth curves. But the location of voltage–time curve gradually decreases with increasing electrolyte concentration. In the electrolyte with more high concentration, much more K^+ is incorporated into ceramic coating by MAO. So the conductance of coating will be increased, and its surface voltage will decrease.

From Fig. 3, in the electrolyte with different concentration, the first break voltage decreases with increasing electrolyte concentration. When the spark begins to appear on the surface of titanium, the voltage is just the first break voltage. By fitting the experimental data, the functional relationship of the first break voltage with electrolyte concentration is obtained. Figure 4 is the concentration of

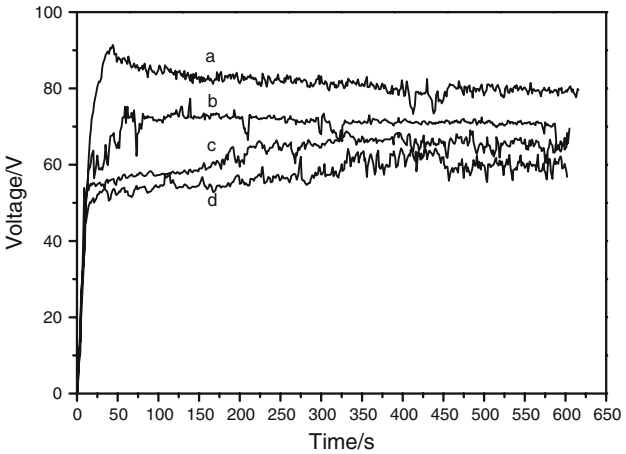

Fig. 3 The voltage–time curve of different concentration of KOH (*a*) 0.6 mol/L, (*b*) 0.8 mol/L, (*c*) 1.0 mol/L, and (*d*) 1.2 mol/L

KOH with the first break–voltage curve on the MAO condition of 400 mA/cm^2. The function is listed as follows:

$$V_B = 166.1 \times \mathrm{Exp}(-C/0.45) + 33.24$$

where V_B is the first break voltage and C is the concentration.

From above equation, the first break voltage decrease with increasing concentration by the form of exponential. Combined with the effect of electrolyte concentration on the composition of coatings, the optimal concentration is 1.0 mol/L.

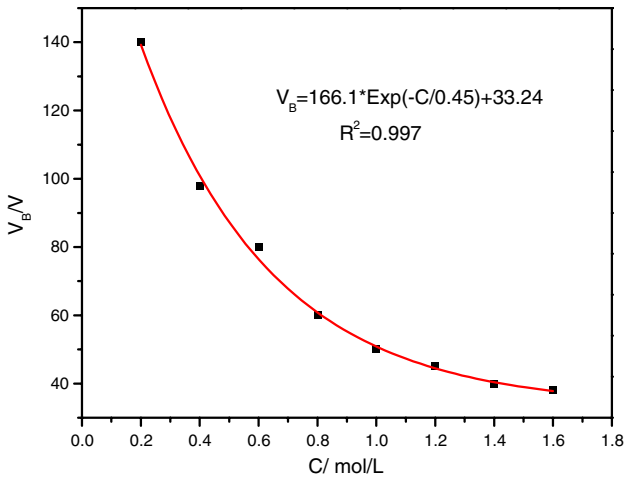

Fig. 4 The concentration of KOH with break–voltage curve on the MAO condition of 400 mA/cm^{-2}

Effect of the current density

Figure 5 shows the XRD patterns of the surface coating phase of samples prepared at different applied MAO current density in the 1.0 mol/L KOH solution. When the applied current density is 150 mA/cm^2 (Fig. 5a), there are only titanium metal and rutile phase XRD peaks, no $K_2Ti_6O_{13}$ phase peak. It is applied that the dielectric breakdown does not occur at low applied MAO current density and only anodic oxidation occurs on the titanium substrate, so only TiO_2 layer is formed on the surface, while no $K_2Ti_6O_{13}$ phase is detected. When the applied current density is 250 mA/cm^2 (Fig. 5b), the $K_2Ti_6O_{13}$ phase XRD peak can obviously be detected. At the same time, the rutile phase and Ti peak intensity begin to increase and decrease, respectively. However, with the further increase of applied current density, the intensity of

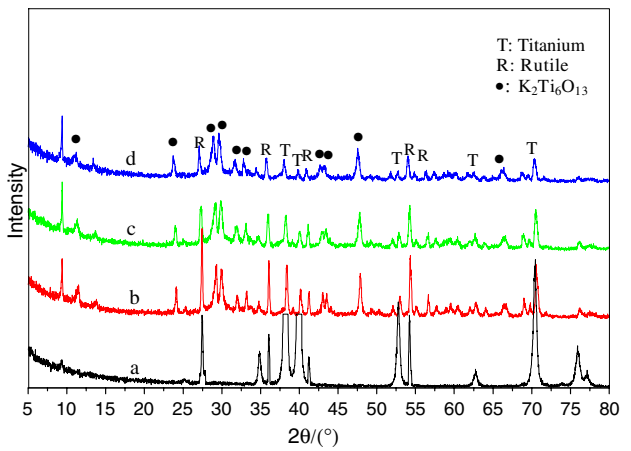

Fig. 5 XRD patterns of the samples oxidized in the 1.0 mol/L KOH solution at the current density of (*a*) 150 mA/cm^2, (*b*) 250 mA/cm^2, (*c*) 400 mA/cm^2, and (*d*) 500 mA/cm^2

rutile phase and Ti XRD peak become weaker, the $K_2Ti_6O_{13}$ phase XRD peak intensity increases slowly, but not apparently, which indicates that increasing applied current density, more titanium metals change into rutile phase, while more rutile phase changes into $K_2Ti_6O_{13}$ phase. The reason is that the dielectric breakdown and reaction speed all are accelerated at higher current density, the grain of formed $K_2Ti_6O_{13}$ phase do not grow up, which lead its low crystallinity. At the same time, the higher current density decreases the time of the dielectric breakdown during which the rutile and $K_2Ti_6O_{13}$ phases are formed.

Figure 6 is the SEM photographs of the samples prepared at different applied current density in the 1.0 mol/L KOH solution. From Fig. 6a, some porous structures can be observed on the surface of coating at low applied MAO current density. The micro pores on the substrate are formed on the area where the micro-arc discharges occurred [20]. With the further increase of applied current density, the porosity is slightly increased, and concentration of whiskers structures strongly increases. When the applied current is 500 mA/cm^2 (Fig. 6c, d), many whiskers structures appear on the coating surface. Correspondingly, these micro pores interweave with whiskers structures on the coating surface.

In the experimental process, the higher the concentration of KOH solution and the applied MAO current density, the faster the voltage reaches the value where the micro-arc discharge appears. The dielectric breakdown occurs more easily. The MAO conditions with different electrolyte concentration of KOH and applied current density are listed in Table 1. From this, the first break voltage and the final voltages which the dielectric breakdown occurred have no relation with the applied current density. When the voltage value only has a little change with time after a period of dielectric breakdown, at this time the voltage is just the final voltage. The two voltages values strongly depend on the concentration and composition of electrolyte [25] and can reflect the properties of electrolyte and preparation status of coatings.

Evaluation of the bioactivity of $K_2Ti_6O_{13}/TiO_2$ bio-ceramic coating

Figure 7 shows the XRD patterns of the surface coating phase of samples (prepared on the condition of 1.0 mol/L KOH solution at 500 mA/cm^2 of applied current density) which are soaked in the biological model fluids for different time. After soaking for two days (Fig. 7b), a very apparent HAp XRD peak is detected at 25.879 of 2θ, which shows some HAp is deposited on the coating surface. With increasing soaking time, the HAp XRD peak intensity becomes stronger, while the XRD peak intensity of rutile

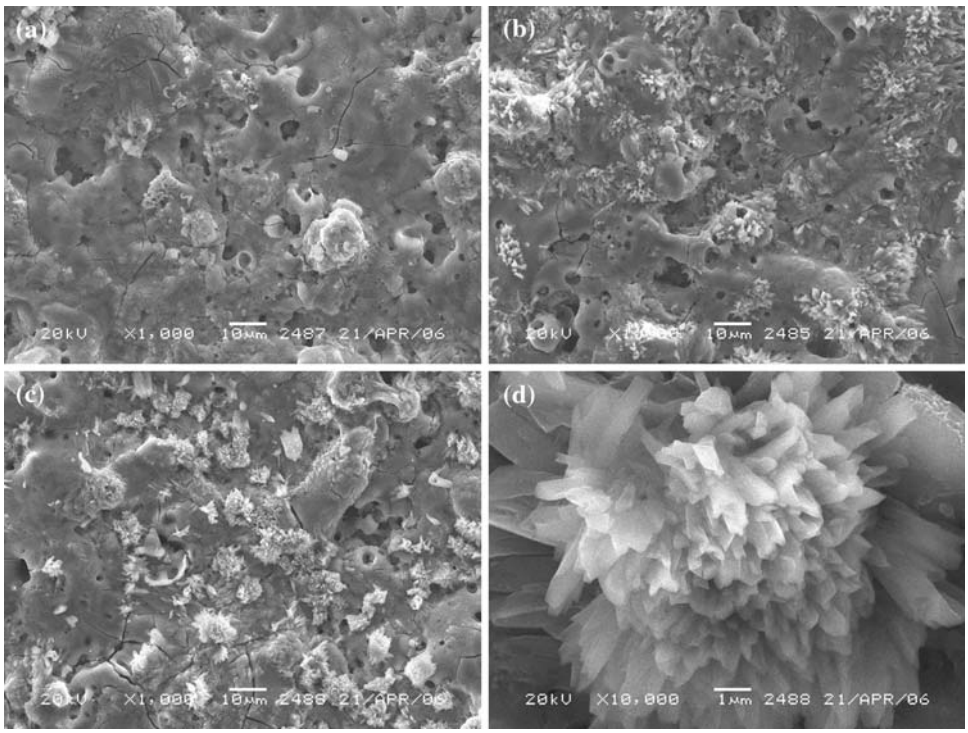

Fig. 6 Surface morphologies of the micro-arc oxidized samples prepared in the 1.0 mol/L KOH solution at the current density of **a** 250 mA, **b** 400 mA, **c** 500 mA, and **d** high magnification of (**c**)

Table 1 The MAO conditions with different electrolyte concentration and applied current density

Electrolyte composition	Applied current density (mA/cm^2)	First-spark voltage (V)	Final voltage (V)
0.6 mol/L KOH	400	76	89
0.8 mol/L KOH	400	65	72
1.0 mol/L KOH	400	58	62
1.2 mol/L KOH	400	50	60
1.0 mol/L KOH	500	58	62
1.0 mol/L KOH	300	58	62
1.0 mol/L KOH	200	58	62

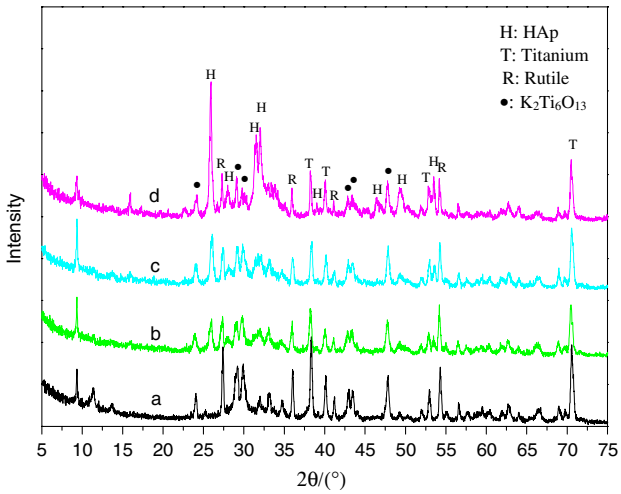

Fig. 7 XRD patterns of the samples (prepared in 1.0 mol/L KOH solution at 500 mA/cm^2 current density) immersed in the biological model fluids for: (*a*) 0 days, (*b*) 2 days, (*c*) 8 days, and (*d*) 12 days

and $K_2Ti_6O_{13}$ phase become weaker and weaker. When the sample is soaked in biological model fluids for 12 days (Fig. 7d), the intensity of HAp XRD peak is much stronger than that soaked for 8 days (Fig. 7c), which indicates that the speed of HAp induced to deposit on the coating surface is accelerated and the thickness of HAp coating becomes great. At the same time, the rutile and $K_2Ti_6O_{13}$ phase XRD peak have been not very apparent. It can be concluded that the predominant composition of coating is HAp phase.

Figure 8 is the SEM photographs of the samples soaked in biological model fluids for different time. Figure 8a shows that there are some spherical structures on the surface of coating, when the sample is soaked in biological model fluids for two days. It's obvious that the spherical structures almost cover the total coating surface. The porous structures existing on the coating surface cannot be observed. The reason is because of the "sheet" structures (Fig. 8d) HAp crystals cover the coating surface. The diameter of the biggest spherical structure is about 10 μm. After soaking for 8 days (Fig. 8b), not only the size of those spherical structures becomes bigger than that soaked for 2 days, but also there are some sheet structures on the surface of spherical structures, which indicates that the spherical structures HAp crystal grows on the coating surface at first, and then the sheet structures HAp crystal

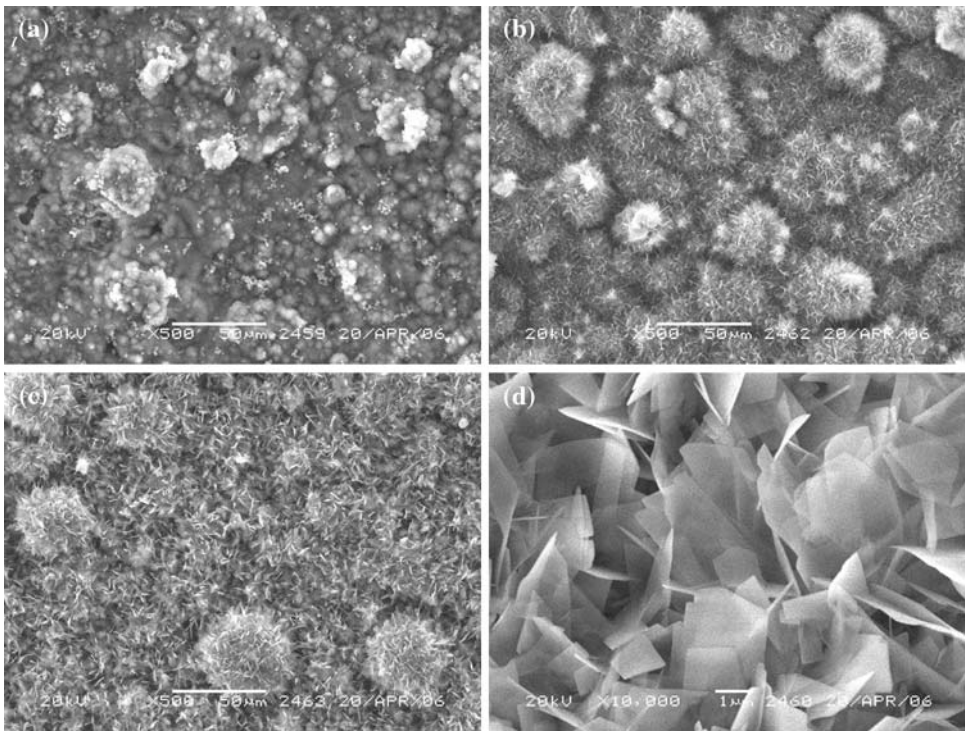

Fig. 8 Surface morphologies of the samples (prepared in 1.0 mol/L KOH solution at 500 mA/cm^2 current density) immersed in the biological model fluids for: **a** 2 days, **b** 8 days, **c** 12 days, and **d** high magnification of sample soaking for 12 days

grows on the surface of spherical structures. When the soaking time reaches 12 days (Fig. 8c), the HAp coating becomes denser and thicker. So there is not any apparent boundary between each HAp crystal on the surface of coating compared with that soaked for 8 days.

The above results show that the $K_2Ti_6O_{13}/TiO_2$ bio-ceramic coating possesses excellent bioactivity, which can easily induce the HAp coating to deposit on its surface soaking in biological model fluids. The excellent HAp-forming ability of the $K_2Ti_6O_{13}/TiO_2$ bio-ceramic coating subjects to its special structure, composition, and physical–chemical properties. First, rutile can adsorb OH^- and PO_4^{3+} from biological model fluids, and also the structure of rutile (101) matches the structure of HAp (0001), the matching structure can be the nuclei for HAp crystal growth [23]. Second, the $K_2Ti_6O_{13}$ phase can be regarded as a kind of compound composed of K_2O and $6TiO_2$ and is an excellent ion exchange substance. When the coating is soaked in biological model fluids, it releases potassium ions from its surface via an exchange with the hydronium ion and Ca^{2+} existing in the fluids [26]. By the ion exchange reaction, a titania hydrogel abundant in Ti–OH groups is formed on its surface. The Ti–OH groups can induce HAp nucleation on the surface of the coating and the increase in the ionic activity product accelerates the HAp nucleation [27, 28]. And some Ca^{2+} exchanges with K^+ and some PO_4^{3+} ions are absorbed from biological model fluids. So a large number of HAp nuclei are formed according to the following equation:

$$10Ca^{2+} + 6PO_4^{2-} + 2OH^- = Ca_{10}(PO_4)_6(OH)_2(HAp) \quad (1)$$

Because the biological model fluids is highly super-saturated to the HAp, once HAp nuclei formed and reached a certain size, it will grow spontaneously up by consuming the Ca^{2+} and PO_4^{3+} of biological model fluids [29]. After some time of soaking, a uniform HAp coating will cover the surface. The deposition process of HAp in the biological model fluids can be described as Fig. 9.

Conclusion

The $K_2Ti_6O_{13}/TiO_2$ bio-ceramic coating has been prepared successfully by micro-arc oxidized on titanium substrate. The composition and surface morphology of coatings change with the increase of applied current density and electrolyte concentration. Only when the current density and electrolyte concentration reach a certain value, the $K_2Ti_6O_{13}$ phase can form on the surface. The best condition of MAO is in 1.0 mol/L KOH electrolyte and at 500 mA/cm^2 of applied current density. After soaking in biological model fluids for 8 days, the HAp coating can be deposited on the surface of samples and cover almost the total surface. It indicates that the $K_2Ti_6O_{13}/TiO_2$ bio-ceramic coating has excellent capability of inducing bone-like apatite in biological model fluids. Compared with other preparation method, the $K_2Ti_6O_{13}/TiO_2$ bio-ceramic

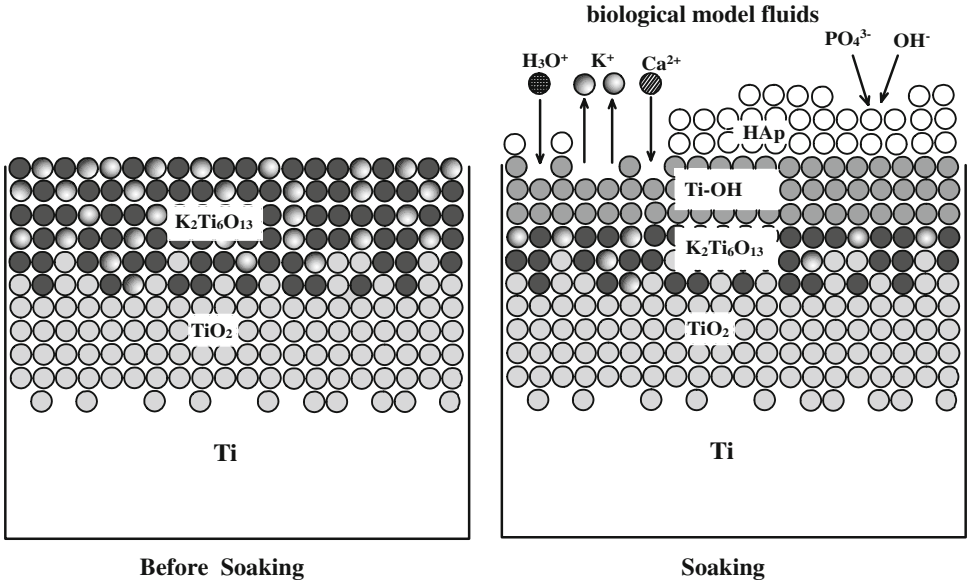

Fig. 9 The process of HAp forming in the biological fluids

coating is prepared by only one step in very gentle condition, its bioactivity is good, and the process is very simple.

Acknowledgement This work was supported by National Science Foundation of China (No. 50674105).

References

1. Zhao ZW, Chen AL, Chen XY, Sun PM, Li HG (2006) Chin J Nonferrous Met 15:2023
2. Han Y, Hong SH, Xu KW (2002) Mater Lett 56:744
3. Zhao ZW, Li HG, Sun PM, Chen XY, Masaazumi O (2005) T Nonferr Metal Soc 15:1368
4. Chen AL, Zhao ZW, Sun PM, Chen XY, Zhang G, Sun ZM (2006) Mater Rev 20:140
5. Nie X, Leyland A, Matthews A (2000) Surf Coat Tech 125:407
6. Zhang YX, Han Y, Huang P, Sun JF, Xu KW (2004) J Chin Ceram Soc 32:122
7. Zhao ZW, Li HG (2002) Rare Metal Cemen Carbi 30:6
8. Frauchiger VM, Schlottig F, Gasser M, Textor M (2004) Biomaterials 25:593
9. Sul YT, Johansson CB, Kang YM, Jeon DG, Albrektsson T (2002) Clin Implan Dent Relat Res 4:78
10. Scherckenbach JP, Marx G, Schlottig F, Textor M, Spencer ND (1999) J Mater Sci-Mater M 10:453
11. Ciobanu G, Carja G, Ciobanu O, Sandu I, Sandu A (2009) Micron 40:143
12. Ducheyne P, Radin S, Heughebaert M, Heughebaert JC (1990) Biomaterials 11:244
13. Ohtsu N, Abe C, Ashino T, Semboshi S, Wagatsuma K (2008) Surf Coat Tech 202:5110
14. Li Y, Lin Q, Chen J, Lan X, Lu C, Li D, Xu Z (2008) Adv Mater Res 47:1351
15. Liu Y, Tsuru K, Hayakawa S, Osaka A (2004) J Ceram Soc Japn 112:634
16. Cui CX, Shen YT, Xu YJ (2003) Rare Metal Mater Eng 32:627
17. Kokubo T (1997) US Patent 5609633
18. Johnson MC (1965) Microelectron Reliab 4:230
19. Yerokhin AL, Nie X, Leyland A, Mattews A (2000) Surf Coat Tech 130:195
20. Li LH, Kong YM, Kim HW, Kim YW (2004) Biomaterials 25:2867
21. Sul YT, Johansson C, Byon E, Albrektsson T (2005) Biomaterials 26:6720
22. Li LZ, Shao ZC, Tian YW, Kang FD, Zhai YC (2004) Corros Sci Prot Tech 16:218
23. Yang B, Uchida M, Kim H (2004) Biomaterials 25:1003
24. Feng QL, Li F, Cui FZ (2002) China Patent No. CN2005 10013523.0
25. Blackwood DJ, Peter LM, Williams DE (1988) Electrochim Acta 33:1143
26. Qi YM, He Y, Cui CX, Liu SJ, Wang HF (2006) Funct Mater 37:1638
27. Kokubo T, Kim HM, Miyaji F (1999) Composites A 30:405
28. Uchida M, Kim HM, Kokubo T (2002) J Biomed Mater Res 63:522
29. Ciobanu G, Carja G, Ciobanu O (2008) Surf Coat Tech 202:2467